Proc. Natl. Acad. Sci. USA
Vol. 91, pp. 7404–7409, August 1994

Review

Dissection of an antibody-catalyzed reaction

Jon D. Stewart, Joseph F. Krebs‡, Gary Siuzdak§, Anthony J. Berdis*, David B. Smithrud*, and Stephen J. Benkovic*¶*

**152 Davey Lab, Department of Chemistry, The Pennsylvania State University, University Park, PA 16802; and Departments of ‡Molecular Biology and §Chemistry, The Scripps Research Institute, 10666 North Torrey Pines Road, La Jolla, CA 92037*

ABSTRACT **Antibody 43C9 accelerates the hydrolysis of a *p*-nitroanilide by a factor of 2.5 × 10^5 over the background rate in addition to catalyzing the hydrolysis of a series of aromatic esters. Since this represents one of the largest rate accelerations achieved with an antibody, we have undertaken a series of studies aimed at uncovering the catalytic mechanism of 43C9. The immunogen, a phosphonamidate, was designed to mimic the geometric and electronic characteristics of the tetrahedral intermediate that forms upon nucleophilic attack by hydroxide on the amide substrate. Further studies, however, revealed that the catalytic mechanism is more complex and involves the fortuitous formation of a covalent acyl-antibody intermediate as a consequence of complementary side chain residues at the antibody-binding site. Several lines of evidence indicate that the catalytic mechanism involves two key residues: His-L91, which acts as a nucleophile to form the acyl-antibody intermediate, and Arg-L96, which stabilizes the anionic tetrahedral moieties. Support for this mechanism derives from the results of site-directed mutagenesis experiments and solvent deuterium isotope effects as well as direct detection of the acyl-antibody by electrospray mass spectrometry. Despite its partial recapitulation of the course of action of enzymic counterparts, the reactivity of 43C9, like other antibodies, is apparently limited by its affinity for the inducing immunogen. To go beyond this level, one must introduce additional catalytic functionality, particularly general acid–base catalysis, through either improvements in transition-state analog design or site-specific mutagenesis.**

Antibodies are capable of catalyzing a variety of chemical transformations (1–5). Antigens have been fabricated that structurally resemble high-energy intermediate species anticipated in a chemical reaction, which can then be used to induce antibodies whose binding energy should stabilize such intermediates or their related transition states along the reaction pathway. For an antibody with a typical 0.1 nM affinity for its antigen and 1 mM affinity for its substrate (defined as the constant for antibody·antigen/substrate dissociation), the difference in the free energy of binding is ≈9.6 kcal·mol^{-1} (1 cal = 4.184 J), which translates to an increase in kinetic turnover of ≈10^7 if all of the difference in binding energy is realized in catalysis. In practice, however, most catalytic antibodies do not efficiently convert this binding energy to catalysis. Consequently, those such as 43C9, the subject of this review, which exhibit large rate enhancements of 10^5–10^6, are of particular interest. The investigation of their mechanism of action is instructive from at least two related points of view: (*i*) what fundamental principles of catalysis are responsible for the rate acceleration, and (*ii*) what features of the transition-state mimic and its complementary antibody site are the primary contributors to catalysis. This information can serve as the basis for obtaining catalytic antibodies possessing high catalytic turnover numbers either through improvements in the design of the eliciting antigen/hapten or through subsequent modifications of the binding site through chemical or genetic methods.

Evidence for Nucleophilic Catalysis by a Catalytic Antibody

Catalytic antibody 43C9 was selected from a panel of 44 antibodies that bound the phosphonamidate transition-state mimic **4** (Scheme I) (6). The intent was to find catalytic antibodies capable of accelerating the hydrolysis of aromatic amide **1**. Amide hydrolysis at slightly alkaline pH involves a putative zwitterionic tetrahedral species—one of several tetrahedral species interconverting through proton transfers and flanked by tetrahedral transition states for their formation and decomposition (7). Phosphonate derivatives have acted as transition-state inhibitors for various esterase enzymes and thus closely mimic the stereoelectronic features of the transition states for hydrolysis of carboxylic esters and amides (8). The antibody 43C9 accelerated hydrolysis of **1** by a factor of 2.5 × 10^5 over the hydrolysis rate measured in the absence of antibody at pH 9.0. By applying transition-state theory, the value of $\Delta\Delta G^\dagger$ is calculated to be −7.5 kcal·mol^{-1} (9). The difference between binding of **1** and **4** to the antibody is an index of the available transition-state binding energy. The binding constant of hapten at pH 9.0 was obtained by titrating the antibody with **4** (monitoring the quenching of intrinsic antibody fluorescence); the K_d value equals 0.8 ± 0.2 nM. The binding constant of **1** at pH 9.0 was obtained from K_m and equals 180 ± 20 μM. The ratio of K_d/K_m provides a $\Delta\Delta G^\dagger$ equal to −7.2 kcal·mol^{-1}. The agreement between the two measures of transition-state stabilization achieved by the catalytic antibody is more than satisfactory. One might conclude from this superficial analysis that the hydrolysis catalyzed by 43C9 proceeds by a simple, one-step mechanism. The experimental facts, however, reveal another story.

The antibody-catalyzed hydrolysis of *p*-nitrophenyl ester **2a** and *p*-nitroanilide **1** has been examined by both pre- and steady-state kinetic techniques (10). The steady-state Michaelis–Menten parameters, k_{cat}/K_m and k_{cat}, as a function of pH are shown in Fig. 1. The data can be fit either to a reaction mechanism involving the titration of a group at the antigen-binding site whose dissociation promotes substrate hydrolysis or to one that features a change in the rate-limiting step around a central antibody-bound intermediate species due to changes in pH. For the *p*-nitrophenyl ester, the rate constant for *p*-nitrophenol release (measured independently) approximates k_{cat} in the pH-independent region (pH > 9). Thus, the apparent pK_a of 9 found for both substrates in the pH rate profiles cannot be due to dissociation of a common acid–base group involved in binding or catalysis. Further support for this conclusion obtains from the absence of pH-dependent binding of **1**, a competitive inhibitor of ester hydrolysis that should be sensitive to the ionization state of an active-site acid–base group. The 10^4 difference in k_{cat} at pH > 9.0 between the two substrates also rules out any mechanism involving a shared conformational change step such as activation of an antibody·substrate complex that is rate-limiting in that region. The pH independence of K_m values for both **1** and **2a** required by the similar pH behavior of k_{cat} and k_{cat}/K_m, however,

Abbreviations: V_H and V_L, heavy-chain and light-chain variable region.

¶To whom reprint requests should be addressed.

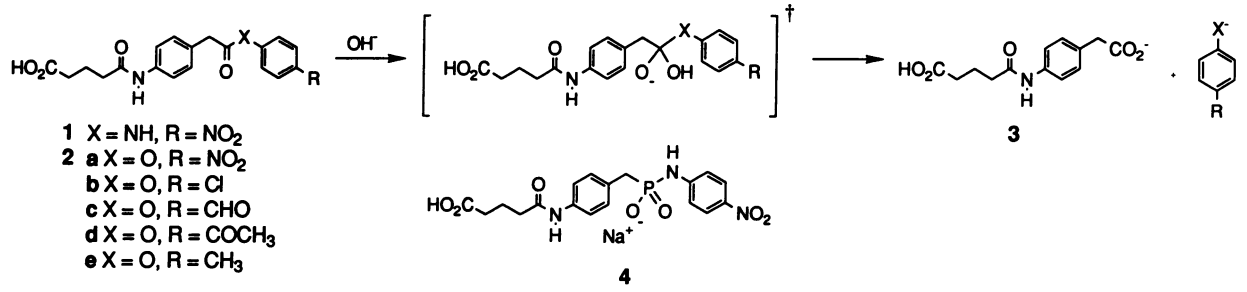

Scheme I

suggests that there is no significant accumulation of the putative intermediate.

Attempts to detect a steady-state intermediate such as an acyl-antibody at low pH (pH 7.0) where its accumulation is more favorable by stopped-flow or rapid-quench methods were unsuccessful (10). Single ^{18}O incorporation into the acid product **3** observed in the presence of $H_2{}^{18}O$ is consistent with an acyl species and definitively rules out a symmetrical tetrahedral intermediate (11). However, using electrospray mass spectrometry, a covalently bound species of mass weight equivalent to an acylated antibody was recently observed at pH 5.9, which represented ≈10% of the total antibody species, thus reinforcing our choice of interpretation. This species was not detected in a similar experiment in the presence of hapten **4**. The data were therefore analyzed by using the kinetic sequence described in Scheme II.

The substrate specificity of 43C9 was further extended to include a series of *p*-substituted phenyl esters **2b–e** (12). Interestingly, little or no reactivity was observed with the corresponding *m*-nitrophenyl ester or anilide or the *p*-chloro-substituted anilide, despite the fact that the *m*-nitro compounds are bound as well as their respective *p*-nitro derivatives. This suggests that a precise, stereochemical orientation of the substrate is necessary within the active site. Since the pH-dependent hydrolysis of esters **2b–e** by 43C9 exhibits k_{cat} and k_{cat}/K_m pH rate profiles similar to the *p*-nitro derivatives, the data were analyzed identically. Values for the estimated rate constants are listed in Table 1.

The pH rate profiles for k_{cat} are thus indicative of a change in rate-limiting step from hydroxide ion-mediated hydrolysis of a steady-state acyl intermediate at low pH to either product release (*p*-nitrophenyl ester) or acylation in the case of esters **1b–e** and the anilide at high pH values. The pH rate profiles for k_{cat}/K_m arise from a similar pH-dependent change from steps involving deacylation to those reflecting acylation. The apparent pK_a observed in the k_{cat}/K_m versus pH rate profiles for the esters shifts from 8.9 (*p*-Cl) to 9.5 (*p*-CH_3) and reflects the small change in k_{-2} consistent with a late transition state in the acylation reaction and, conversely, attenuation of the substituent effect in the reverse deacylation. Note that the limitation of rate-limiting product release imposed by *p*-nitrophenol is relieved by changing the *p* substituent, although the advantage is offset by a slower acylation rate.

The rates of the antibody-catalyzed acylation (k_2) for this series of substrates correlate with σ, affording a ρ value of +2.3. In contrast, a similar correlation for the hydrolysis rates for the same esters in the absence of antibody provides a ρ value of +0.8 (12). For comparison, hydrolysis of phenyl esters via a general base mechanism or by nucleophilic attack by hydroxide ion is characterized by ρ values as low as 0.5–0.7 (13, 14) to 1.0–1.2 (13, 15, 16), respectively. The large ρ value observed for the antibody-catalyzed reaction is more characteristic of nucleophilic attack and expulsion of a charged leaving group by a nitrogen nucleophile, such as imidazole (13–15). Thus, the substituent effect provides further support for an acyl intermediate and against a one-step general base or nucleophilic attack mechanism for hydrolysis. The inability of 43C9 to protonate its leaving group is underscored by the dramatic 80-fold decrease in k_{cat} estimated for the *p*-chloroanilide species.

Collectively from the kinetic and thermodynamic binding measurements, a free energy reaction coordinate diagram was constructed for hydrolysis of the *p*-nitro-substituted ester and anilide (Fig. 2) (10). There are several striking features of the two reaction profiles. One is the high stability of the antibody Ab·P_1·P_2 complex, which has a ΔG equal to 7–12 kcal·mol^{-1} lower than the respective uncomplexed substrates. This tight product complex ultimately limits the rate of ester hydrolysis at high pH. The second noteworthy feature is the increased kinetic barrier for the formation of Ab·I from the amide relative to the ester substrate so that this step ultimately limits amide turnover by the antibody at high pH. This free energy profile may provide a glimpse of how nonoptimized enzymes may have functioned with their efficiency of turnover hampered by the unevenness in the ΔG barriers for the various ground states and their respective transition states. We will return to a more direct comparison of 43C9 to an esterase enzyme later, but the remarkable finding to emphasize now is how far the mechanism of action of 43C9 has departed from the simple hydrolysis implicit in the original hapten design. One simple rationale is that covalent active site chemistry becomes more probable the higher the affinity of the antibody for the transition-state mimic, provided that nucleophilic side chains are made available through a requirement for charge neutralization or hydrogen bonding in hapten binding.

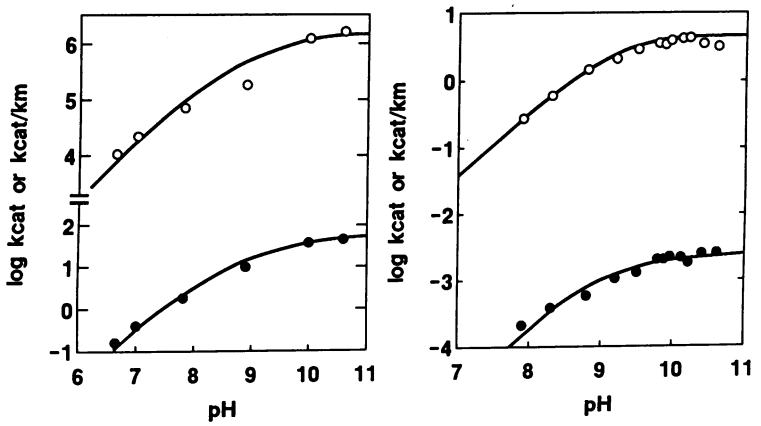

FIG. 1. pH rate profiles for 43C9-catalyzed hydrolysis of *p*-nitrophenyl ester **2a** (*Left*) and *p*-nitroanilide **1** (*Right*).

Construction of the 43C9 Model Structure

Recent mechanistic studies of 43C9 have made use of site-directed mutagenesis to

$$Ab + S \underset{k_{-1}}{\overset{k_1}{\rightleftharpoons}} Ab{\cdot}S \underset{k_{-2}}{\overset{k_2}{\rightleftharpoons}} Ab{\cdot}I \xrightarrow{k_3[OH^-]} Ab{\cdot}P_1{\cdot}P_2 \underset{k_{-4}}{\overset{k_4}{\rightleftharpoons}} Ab{\cdot}P_2 + P_1 \underset{k_{-5}}{\overset{k_5}{\rightleftharpoons}} Ab + P_2$$

Scheme II

probe the roles of individual residues involved in binding and catalysis. These experiments were guided by the previously discussed kinetic studies as well as a computer model of the 43C9 Fv fragment with bound ligands (17). Computer modeling of antibody variable (V) regions takes advantage of both the modular nature of antibody structures as well as the high degree of conservation of tertiary structure between antibodies with widely divergent binding specificities. The 43C9 model was constructed in several steps using the previously published Antibody Structural data base (18, 19). Briefly, sequence comparisons were used to select the framework regions, then the complementarity-determining loops were constructed, and finally the V_L (L, light chain) and V_H (H, heavy chain) regions were paired. The first step was to compare the primary sequence of the L and H chains of 43C9 with those of antibodies whose three-dimensional structures are known. For 43C9, the L chain most resembled that of the anti-phosphorylcholine antibody McPC603, while the H chain of 43C9 was most similar to that of the anti-lysozyme antibody D1.3. These data base sequences were then modified to match those of 43C9. The H3 loop is the most difficult to model as a result of its high diversity in sequence and length, and the likely conformation of the 43C9 H3 loop was determined by a series of steps after examining both the V_L/V_H interface and the binding of antigen (see below).

Once constructed, the antibody model revealed a T-shaped cleft for the antigen-binding region. The side chain of Arg-L96 is located at the vertex of the T, where it is situated to form a salt bridge with the negatively charged phosphonamidate group of the hapten. Such interactions have previously been observed in antibodies and other proteins that bind phosphorus oxyanions (for example, see refs. 20 and 21). Once docked in this position, the hapten fits snugly into the antigen-binding pocket. Furthermore, this binding mode clarifies the position of the H3 loop, since only a few conformations are available that do not involve extensive steric clashes with the protein or antigen. The amide substrate was docked analogously (Fig. 3) (22). The *p*-nitrophenyl portion of the substrate lies within a cleft whose walls are formed by Tyr-L32 and the -H3 loop with the side chain of Arg-H100A positioned to form a polar hydrogen bond with the nitro group of the hapten. The acyl portion lies on top of the side chain of Trp-H52 and has extensive contacts with the H1 and H2 loops.

The computer model has provided a number of insights into the catalytic mechanism of 43C9. The proximity of the substrate carbonyl to residues His-L91, Arg-L96, and Tyr-H95 suggested that these residues play roles in catalysis. Specifically, the N^{δ} of His-L91 is located ≈4.5 Å from the carbonyl carbon of the substrate. On the other hand, the side chain of the other active site histidine (His-H35) is >7 Å from the substrate carbonyl, too far for this imidazole to act as a nucleophile. The side chain of His-H35, moreover, is involved in an extensive hydrogen bonding network at the bottom of the antigen-binding pocket, suggesting that this residue plays a structural role in maintaining the conformation of the binding pocket. The hydroxyl of Tyr-H95 appears to hydrogen bond with one of the oxygens of the hapten; this proximity suggested its involvement along with Arg-L96 in stabilizing the tetrahedral intermediates or transition states. The accuracy of the model will ultimately be tested by x-ray crystallography, but to date its predictions have proven remarkably accurate (see below).

Application of the Proton Inventory Technique to Antibody Catalysis

As probes of enzyme mechanisms, the solvent isotope effect and proton inventory have found their greatest use with the serine proteases (23). This technique was used to further evaluate the proposed catalytic mechanism of 43C9, fleshed out in view of the modeled antibody–substrate complex (Fig. 3). Proton inventories of k_{cat} and k_{cat}/K_m at pL 8 are bowed downward for the 43C9-catalyzed hydrolysis of *p*-chlorophenyl ester **2b**. At this pL value, breakdown of the acyl-antibody intermediate represents the rate-limiting step. A bowed downward proton inventory can most easily be interpreted in terms of a mechanism involving the transfer of two or more protons in a single rate-limiting transition state (24)—in this case, breakdown of the tetrahedral intermediate by hydroxide ion attack on the putative acyl-imidazole. Since the pK_a for the tetrahedral intermediate species is close to that of Arg-L96 [the pK_a for an analogous tetrahedral intermediate is ≈12.9 (25)], Arg-L96 either transfers a proton to the negatively charged oxygen of the tetrahedral intermediate or is involved in strong hydrogen bonding interactions with the oxygen. The second proton observed from the proton inventory likely arises from a proton transfer to the imidazole of the His nucleophile. At pL 9.5, a solvent isotope effect of ≈1.2 on k_{cat}/K_m is obtained for the 43C9-catalyzed hydrolysis of *p*-chlorophenyl ester **2b**. For all intents and purposes, this is most likely not a solvent isotope effect on the acylation step of the reaction but instead reflects a viscosity effect on substrate binding. All of these solvent isotope effects are consistent with the change in rate-limiting steps required by the kinetic sequence of Scheme III.

Table 1. Kinetic parameters for *p*-substituted ester hydrolysis by antibody 43C9 at pH 9.3

R	k_{cat}, s^{-1}	K_m, μM	k_1, $\mu M \cdot s^{-1}$	k_{-1}, s^{-1}	k_2, s^{-1}	k_{-2}, s^{-1}	k_5, s^{-1}
NO_2	≈25	53	1.3	25 ± 4	≥180	≥3600	40 ± 5
CH_3CO	≈0.87	≈3000		No value	≈1.7	≥1400	>700
CHO	1.0 ± 0.1	250 ± 80					
Cl	1.7 ± 0.2	720 ± 220	0.15	89 ± 6	≈2.2	≥1200	≈900
CH_3	0.15 ± 0.03	≈3000			≈0.25	≥1900	>600

k_3 (60 $\mu M \cdot s^{-1}$) and k_4 (330 ± 40 s^{-1}) are assumed to be constant for all substrates since the acyl portion is identical in all substrates. Data are from Gibbs *et al.* (12).

Probing the Active Site of 43C9 by Mutagenesis

Using the single-chain Fv version of 43C9, which retains the kinetic parameters of the parent monoclonal antibody (26), a series of site-directed mutagenesis studies were undertaken. The His-L91 to Gln (H-L91-Q) mutant, which retains a degree of hydrogen bonding but no nucleophilic capability, possessed no detectable catalytic activity when assayed against the *p*-chlorophenyl ester substrate **2b** (22). This finding reflects at least a 50-fold decrease in catalytic activity. On the other hand, the affinity of this mutant for ligands is essentially unchanged from that of the wild type (Table 2). The results of the binding assays demonstrated that the lack of observed catalysis was not due to large changes in antibody structure or to a lack of substrate binding. Hapten binding was used as a surrogate for substrate binding because of the rapid spontaneous hydrolysis of the ester substrates and the weak binding of anilide **1**. Measurement of the binding affinity for the hydrolysis products, acid **3** and *p*-nitrophenol, which correspond to each arm of the L-shaped hapten, takes advantage of the strong binding of these products to localize changes in hapten binding to one region of the combining site. Collectively, these observations support a role for His-L91 as the nucleophile in catalysis. Moreover, no covalent intermediate was detected by electrospray mass spectrometry when the

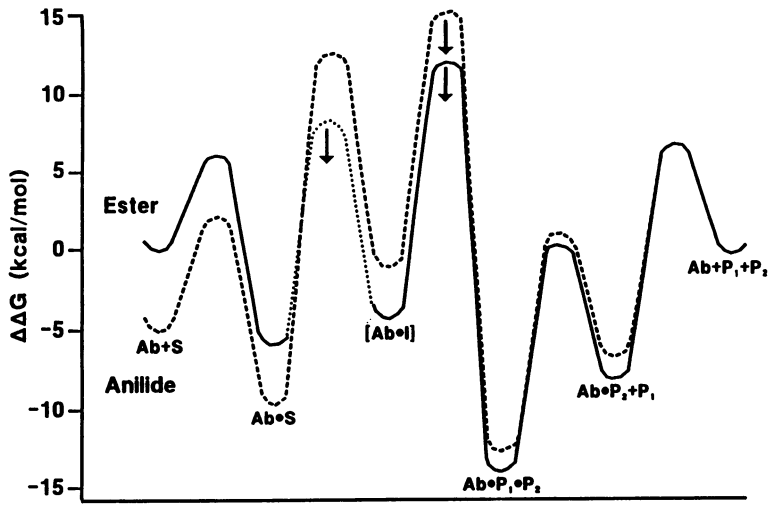

FIG. 2. Reaction ΔG profile for hydrolysis of *p*-nitrophenyl ester **2a** (——) and *p*-nitroanilide **1** (- - -) by 43C9 at pH 7. Ground state energy of amide **1** was set 5 kcal·mol^{-1} below that of the arbitrary value for ester **2a**. Free energies of the products were set to 0 kcal·mol^{-1} and standard states of all substrates and products are 1 M. Arrows show that transition states are set at their highest values, based on the estimated rate constants.

H-L91-Q mutant was incubated with *p*-nitrophenyl ester **2a**. Substitution of Ser or Glu for His-L91 gave mutants with no appreciable activity, despite their ability to bind ligands. Substitution of a Cys residue at position L91 apparently interferes with the formation of the V_L intrachain disulfide bond involving the naturally occurring Cys residues at L23 and L88 since no folded protein was recovered (J.D.S., V. A. Roberts, E. D. Getzoff, and S.J.B., unpublished data).

Substitution of Arg-L96 with Gln removes the positive charge while retaining some hydrogen bonding ability. The R-L96-Q mutant is catalytically inactive, supporting a role for this residue in catalysis. In addition, the affinity of this mutant for the hapten was reduced some 20-fold, while the affinity for the other ligands was relatively unaffected (17). These results support the notion that the side chain of Arg-L96 interacts specifically with the phosphonamidate, since it is this group that distinguishes the hapten from either of the products. Substitution of His for Arg-L96 gave a mutant (R-L96-H) that lacked catalytic activity. Moreover, its affinity for all ligands decreased substantially, suggesting some reorganization of the antigen-binding pocket to accommodate the larger side chain, which is consistent with the tight packing of side chains of the amino acids that form the floor of the antigen-binding site (M. W. Crowder, J.D.S., V. A. Roberts, E. D. Getzoff, and S.J.B., unpublished data). Substitution of His-H35 with Asn or Phe also appears to disrupt the active site structure, as evidenced by their decreased affinities for the various ligands (22). Finally, to probe the role of the hydroxyl of Tyr-H95 in transition-state binding, this residue was changed to Phe. The Y-H95-F mutant possessed ≈50% of the wild-type activity, in accord with the pH rate profiles obtained for the wild-type 43C9, which did not exhibit involvement of a dissociable Tyr residue (22).

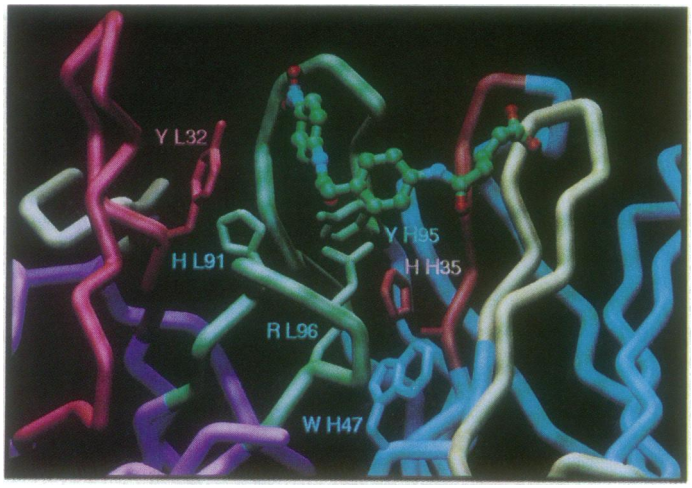

FIG. 3. Model of 43C9 Fv fragment with bound amide substrate. Selected residues that line the antigen-binding site are highlighted. The V_L segment is on the left and the V_H segment is on the right. His-L91, the putative nucleophile, lies near the scissile carbonyl of the substrate and Arg-L96 is poised to act as an oxyanion hole. The hydroxyl of Tyr-H95 lies near the carbonyl oxygen, while the side chain of Tyr-L32 forms one wall of the antigen binding pocket.

Attempts to Improve the Catalytic Efficiency of 43C9

We have explored the possibility of introducing residues to accomplish the protonation of either the leaving group or the tetrahedral species in order to lower the free energy requirements during passage along the reaction coordinate. The proximity of Tyr-L32 to the leaving group suggested that substituting this residue with one capable of proton transfer might accomplish our goal. Replacement of Tyr-L32 with His or Glu provided no observable increase in hydrolysis of the *p*-chlorophenyl ester substrate at pH 7–8.5, where the acylation step is mainly rate-limiting (ref. 22; J.D.S., D.B.S., V. A. Roberts, E. D. Getzoff, and S.J.B., unpublished data). This indicates that the side chain is improperly positioned for proton donation or, in the case of the His residue, its pK_a is below pH 7. The latter is a strong possibility because of the electropositive environment of the antigen-binding site, resulting from Arg residues at positions L96 and H100A. Similarly, the side chain of Tyr-H95 is located near the scissile carbonyl and also provides an opportunity for proton donation to the tetrahedral species. Unfortunately, the Y-H95-H mutation decreased substrate binding to the extent that only the *p*-nitrophenyl ester was useful as a substrate due to solubility limitations. For this substrate at pH 7.45, where deacylation is rate-limiting, the k_{cat} value of the mutant was reduced 4-fold relative to that of the wild type (22).

A carboxylate side chain was placed adjacent to the N^{ϵ} of His-L91 by substituting Glu for Gln-L89. We anticipated that the resulting hydrogen bond would help orient the N^{δ} of His-L91 for nucleophilic attack and might also facilitate proton transfer. Unfortunately, the Q-L89-E mutant displayed only ≈50% of the wild-type activity (J.D.S., V. A. Roberts, E. D. Getzoff, and S.J.B., unpublished data). Collectively, these results underscore the exacting constraints that must be satisfied to improve turnover.

Our final approach to rationally improve catalysis by 43C9 was to increase product release since this step is rate-limiting for *p*-nitrophenyl ester hydrolysis at high pH values. As noted above, the side chain of Arg-H100A is positioned to form a charged hydrogen bond with the nitro group of the hapten. Presuming that this hydrogen bond might be at least

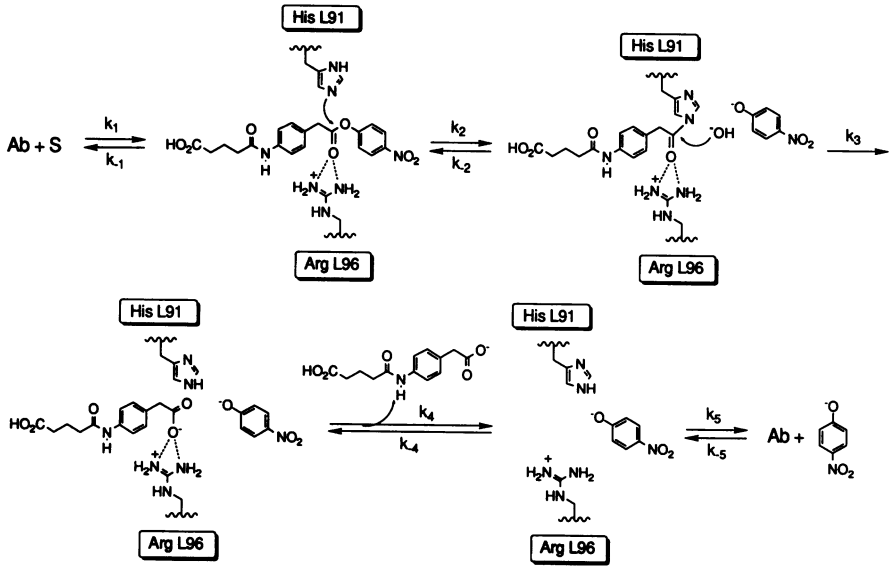

Scheme III

partially responsible for slow product release, Arg-H100A was replaced with Gln. Thermodynamic binding measurements indicated that the affinity of the R-H100A-Q mutant for *p*-nitrophenol had been reduced 4.3-fold relative to that of the wild type. Furthermore, direct measurements of the on and off rates for *p*-nitrophenol binding to this mutant (22 $\mu M \cdot s^{-1}$ and 103 s^{-1}, respectively) indicated that the off rate was increased 2.5-fold relative to the wild type. This increased off rate was manifested by a k_{cat} value of 100 s^{-1} for the *p*-nitrophenyl ester substrate at pH 10, 2.5-fold higher than that for the wild-type antibody in the pH-independent region (D.B.S., V. A. Roberts, E. D. Getzoff, and S.J.B., unpublished data). This provides an example of a means for relieving product inhibition without deleterious effects on the overall turnover of the antibody.

Comparison of the Mechanism of 43C9 with Those of Analogous Enzymes

From the outset, our goal has been to produce antibody catalysts whose efficiencies match those of highly evolved enzymes. This invites two questions: (*i*) to what extent have we succeeded in producing effective catalysts, and (*ii*) to what extent do catalytic antibodies resemble their enzymic counterparts? Antibody 43C9 is a potent catalyst for anilide and ester hydrolysis at pH > 9.0, with k_{cat} values within a factor of 25 and 2, respectively, of chymotrypsin at pH 7.0 (10). By this criterion, then, we have succeeded in producing a catalyst with remarkable activity.

Mechanistic studies of 43C9 have shown that an antibody whose evolution has been directed toward tighter binding of a transition-state analog can recapitulate a number of characteristics of an enzyme whose evolution has been directed by increased catalytic efficiency. Covalent catalysis allows a difficult chemical transformation to be broken into more manageable units and represents a common theme in enzyme-catalyzed amide hydrolysis. The use of a His residue as the nucleophile, however, appears to be unprecedented. On the other hand, this participation is reasonable since His and Tyr (27) are the only residues acting in the absence of general acid–base catalysis that might be expected to reversibly form acyl-antibody intermediates. Nature has circumvented this problem in enzymes by constructing multiresidue networks involving general base catalysis; for example, the Cys–His ion pair in the case of subtilisin or the catalytic triad of the serine proteases. The use of an oxyanion hole to stabilize the tetrahedral transition states and intermediates has also been reproduced by 43C9. In the case of carboxypeptidase A, which also employs an Arg residue in this role, this interaction contributes 6–8 $kcal \cdot mol^{-1}$ to transition-state stabilization (28). Unfortunately, we were unable to measure the contribution in free energy of Arg-L96 to transition-state stabilization in the case of 43C9 since the catalytic activity of the R-L96-Q mutant was below our detection limits.

Concluding Remarks

How can the lessons learned from studies of 43C9 be applied to creating more effective antibody catalysts? First, our results have underlined the importance of high affinity for the transition-state analog, provided that the antigen accurately represents the transition state for a given reaction. It is worth noting that no 43C9 mutant whose K_d for the transition-state analog was >1 nM displayed catalytic

Table 2. Thermodynamic dissociation constants for ligand binding and steady-state kinetic parameters for *p*-chlorophenyl ester hydrolysis at pH 8.5 and 25°C by wild-type and mutant 43C9 single-chain antibodies

	K_d			Kinetic parameters	
Protein	Hapten, nM	Acid, μM	Phenol, μM	k_{cat}, s^{-1}	K_m, μM
Wild type	≤1	15 ± 1	0.6 ± 0.1	0.46 ± 0.05	470 ± 160
Y-L32-H*	0.67 ± 0.35	12 ± 3	0.38 ± 0.09	0.17 ± 0.01	1300 ± 100
Y-L32-E‡	≤2	15 ± 3	4.3 ± 0.4	NA	NA
Q-L89-E‡	≤2	16 ± 3	0.64 ± 0.21	0.22 ± 0.02	1700 ± 200
H-L91-Q*	≤1	17 ± 3	0.53 ± 0.16	NA	NA
H-L91-S‡	≤1	24 ± 4	2.0 ± 0.3	SA	SA
H-L91-E‡	360 ± 10	>200	12 ± 1	NA	NA
H-H35-N*	16 ± 2	100 ± 10	5.5 ± 1.5	NA	NA
H-H35-F*	13 ± 6	15 ± 2	1.4 ± 0.1	NA	NA
R-L96-Q§	16 ± 2	31 ± 8	0.96 ± 0.16	NA	NA
Y-H95-F*	≤2	25 ± 8	0.65 ± 0.22	0.18 ± 0.01	990 ± 90
Y-H95-H*	≤2	21 ± 6	0.70 ± 0.18	NA	NA
R-H100A-Q¶	≤1	15 ± 3	2.6 ± 0.5	ND	ND

NA, no detectable catalytic activity; SA, slight activity; ND, not determined.
*Data are from Stewart *et al.* (22).
‡J.D.S., V. A. Roberts, E. D. Getzoff, and S.J.B., unpublished data.
§Data are from Roberts *et al.* (17).
¶D.B.S., V. A. Roberts, E. D. Getzoff, and S.J.B., unpublished data.

activity. This further underscores the importance of hapten design, in particular the nature of the functional group that mimics the reactive moiety in the substrate (29, 30). Anionic phosph(or/on)yl ligands have been shown to accurately mirror the transition states for enzymes that cleave amides, and this has been quantitatively demonstrated for both β-lactamase (31) and carboxypeptidase A (28). As we (32) and Jacobs (33) have shown, this relationship also holds for antibody catalysis, where a direct correlation exists between the affinity of an antibody for the transition-state analog and its catalytic efficiency. As a result, the most effective antibody catalysts will be those with the highest binding affinity for hapten. Methods that provide antibodies whose affinities for the transition-state analog are ≤1 nM are therefore crucial to isolating efficient catalysts. Recent advances in cloning and screening large combinatorial libraries of antibody genes should prove useful in this search (34), especially since they permit randomly mutated antibody genes to be selected for higher binding affinity. This approach alone, however, may be insufficient to incorporate general acid–base catalysis into the mechanism (the major deficiency of the 43C9 mechanism) unless these hydrogen bonding interactions can be made to measurably contribute to antigen binding. Rather, it may be necessary to install the required residues later by protein engineering techniques unless rules are shown to exist that predict the nature of the antigen-binding site residues in response to structural elements within the hapten (35).

While a useful guide, the relationship between antigen binding and catalytic efficiency is limited if one wishes to use existing antibodies as a platform for creating catalysts with altered specificities. In this case, the new transition states are not likely to be well-represented by the original antigen and the relationship that $K_d/K_m = k_{cat}/k_{uncat}$ is likely to break down. In a practical sense, this means that binding affinity alone may not be a useful means for selecting potential catalysts; rather, such candidates must be directly screened for their catalytic activity. Expressing antibody genes in microorganisms and using the antibody-catalyzed reactions to provide metabolites required for growth holds considerable promise (36), although a generic screen using surface ionization techniques may eventually prove feasible (37).

We are pleased to acknowledge the fruitful collaboration with Victoria A. Roberts and Elizabeth D. Getzoff (The Scripps Research Institute) that led to their construction of the computer model of the 43C9 Fv fragment. This work was partially supported by grants from the Office of Naval Research (N00014-91-J-1593), a postdoctoral fellowship from the Helen Hay Whitney Foundation (J.D.S.), and a postdoctoral fellowship from the National Institutes of Health (D.B.S.; GM 15536-02).

1. Stewart, J. D. & Benkovic, S. J. (1993) *Drug News Perspect.* **6**, 522–531.
2. Stewart, J. D. & Benkovic, S. J. (1993) *Intern. Rev. Immunol.* **10**, 229–240.
3. Benkovic, S. J. (1992) *Annu. Rev. Biochem.* **61**, 29–54.
4. Lerner, R. A., Benkovic, S. J. & Schultz, P. G. (1991) *Science* **252**, 659–667.
5. Hilvert, D. (1992) *Pure Appl. Chem.* **64**, 1103–1108.
6. Janda, K. D., Schloeder, D., Benkovic, S. J. & Lerner, R. A. (1988) *Science* **241**, 1188–1191.
7. Bruice, T. C. & Benkovic, S. J. (1966) *Bioorganic Mechanisms* (Benjamin, New York), Chapt. 1.
8. Wolfenden, R. (1972) *Acc. Chem. Res.* **5**, 10–18.
9. Benkovic, S. J., Napper, A. D. & Lerner, R. A. (1988) *Proc. Natl. Acad. Sci. USA* **85**, 5355–5358.
10. Benkovic, S. J., Adams, J. A., Borders, C. L., Jr., Janda, K. D. & Lerner, R. A. (1990) *Science* **250**, 1135–1139.
11. Janda, K. D., Ashley, J. A., Jones, T. M., McLeod, D. A., Schloeder, D. M., Weinhouse, M. I., Lerner, R. A., Gibbs, R. A., Benkovic, P. A., Hilhorst, R. & Benkovic, S. J. (1991) *J. Am. Chem. Soc.* **113**, 291–297.
12. Gibbs, R. A., Benkovic, P. A., Janda, K. D., Lerner, R. A. & Benkovic, S. J. (1992) *J. Am. Chem. Soc.* **114**, 3528–3534.
13. Bruice, T. C. & Mayahi, M. F. (1960) *J. Am. Chem. Soc.* **82**, 3067–3071.
14. Bruice, T. C. & Benkovic, S. J. (1964) *J. Am. Chem. Soc.* **85**, 1–8.
15. Bruice, T. C. & Schmir, G. L. (1957) *J. Am. Chem. Soc.* **79**, 1663–1667.
16. Kirsch, J. F., Clewell, W. & Simon, A. (1968) *J. Org. Chem.* **33**, 127–132.
17. Roberts, V. A., Stewart, J. D., Benkovic, S. J. & Getzoff, E. D. (1994) *J. Mol. Biol.* **235**, 1098–1116.
18. Getzoff, E. D., Tainer, J., Lerner, R. A. & Geysen, H. M. (1988) *Adv. Immunol.* **43**, 1–98.
19. Roberts, V. A., Iverson, B. L., Iverson, S. A., Benkovic, S. J., Lerner, R. A., Getzoff, E. D. & Tainer, J. A. (1990) *Proc. Natl. Acad. Sci. USA* **87**, 6654–6658.
20. Glockshuber, R., Stadlmüller, J. & Plückthun, A. (1991) *Biochemistry* **30**, 3049–3054.
21. Davies, D. R., Padlan, E. A. & Sheriff, S. (1990) *Annu. Rev. Biochem.* **59**, 439–473.
22. Stewart, J. D., Roberts, V. A., Thomas, N., Getzoff, E. D. & Benkovic, S. J. (1994) *Biochemistry* **33**, 1994–2003.
23. Venkatasubban, K. S. & Schowen, R. L. (1985) *CRC Crit. Rev. Biochem.* **17**, 1–44.
24. Schowen, K. B. & Schowen, R. L. (1982) *Methods Enzymol.* **87**, 551–606.
25. Fox, J. P. & Jencks, W. P. (1974) *J. Am. Chem. Soc.* **96**, 1436–1448.
26. Gibbs, R. A., Posner, B. A., Filpula, D. R., Dodd, S. W., Finkelman, M. A. J., Lee, T. K., Wroble, M., Whitlow, M. & Benkovic, S. J. (1991) *Proc. Natl. Acad. Sci. USA* **88**, 4001–4004.
27. Martin, M. T., Napper, A. D., Schultz, P. G. & Rees, A. G. (1991) *Biochemistry* **30**, 9757–9761.
28. Phillips, M. A., Kaplan, A. P., Rutter, W. J. & Bartlett, P. A. (1992) *Biochemistry* **31**, 959–963.
29. Liotta, L. J., Benkovic, P. A., Miller, G. P. & Benkovic, S. J. (1993) *J. Am. Chem. Soc.* **115**, 350–351.
30. Stewart, J. D., Liotta, L. J. & Benkovic, S. J. (1993) *Acc. Chem. Res.* **26**, 396–404.
31. Rahil, J. & Pratt, R. F. (1994) *Biochemistry* **33**, 116–125.
32. Stewart, J. D. & Benkovic, S. J. (1993) *Chem. Soc. Rev.* **22**, 213–219.
33. Jacobs, J. W. (1991) *Bio/Technology* **9**, 258–262.
34. Posner, B., Lee, I., Itoh, T., Pyati, J., Graff, R., Thornton, G. B., La Polla, R. & Benkovic, S. J. (1993) *Gene* **128**, 111–117.
35. Posner, B., Smiley, J., Lee, I. & Benkovic, S. (1994) *Trends Biochem. Sci.* **19**, 145–150.
36. Tang, Y., Hicks, J. B. & Hilvert, D. (1991) *Proc. Natl. Acad. Sci. USA* **88**, 8784–8786.
37. Brummel, C. L., Lee, I. N. W., Zhou, Y., Benkovic, S. J. & Winograd, N. (1994) *Science* **264**, 399–402.